# Seismic wave simulation in poro-viscoelastic hot rocks

Biancamaria Farina[1], Flavio Poletto[1], José M. Carcione[1]

[1] Istituto nazionale di oceanografia e di geofisica sperimentale - OGS, Borgo Grotta Gigante 42/c, 34010 Sgonico (Trieste), Italy

bfarina@inogs.it

**Keywords:** Brittle, ductile, supercritical, Burgers model, Gassmann theory, seismic-wave simulation.

## ABSTRACT

Seismic-wave modelling is a key tool to characterize the Earth's structure, nearby geothermal areas where the presence of high temperatures can cause the existence of supercritical fluids and also partial melting. The seismic characterization of these areas is very important especially in deep drilling and high-enthalpy systems. Carcione and Poletto (2013) study the seismic properties variations in the presence of a transition between zones with brittle and ductile behaviour. Carcione et al. (2014) propose an algorithm, based on the Burger mechanical model, to simulate full-waveform propagation in this areas.

The presented full-wave solver is based on the Burger mechanical model, which allows us to describe the anelastic behaviour due to shear deformation and plastic flow, and the Gassmann equation to account for the fluid properties in the poro-viscoelastic model. The shear viscosity that relates the stiffness components of the brittle and ductile formation to temperature, is calculated by the Arrhenius equation and the octahedral-stress criterion. The algorithm is based on a direct grid method, and the equations of motion are solved in the time domain by using memory variables (Carcione 2014), spatial derivatives and time integration are obtained with Fourier pseudo-spectral method and Runge-Kutta technique, respectively.

We present synthetic seismograms recorded, along a vertical seismic profile (VSP), in wet and dry viscoelastic media characterized by different temperature profiles, in order to analyse the observability of the associated variations by borehole seismic methods (Poletto and Miranda, 2004).

## 1. INTRODUCTION

Seismic waves can provide important information, useful to characterize the Earth's structure in particular nearby the transition zone between the brittle and the ductile part of the crust (BDT), the geothermal areas and the magmatically active areas. In these regions, temperatures can be higher than the critical temperature of water implying the possible presence of supercritical fluids.

Carcione and Poletto (2013) proposed an elastic-plastic rheology to model the BDT. They introduced a stress-strain relation including the effect of crust anisotropy, seismic attenuation and ductility to model the deformation on the basis of the shear modulus variations related to temperature.

Carcione et al. (2014) proposed a full-waveform algorithm, based on the Burger mechanical model and the Arrhenius equation to calculate the flow viscosity, to model temperature-dependent propagation of seismic waves in geothermal and magmatic crustal areas.

Carcione et al. (2016) extended the theory and the simulation algorithm considering the poro-viscoelastic case. They explicitly modelled the effects of saturating fluids, generally water and steam at various pressure-temperature conditions also considering the possible supercritical behaviour. The full-wave solver is based on the Burgers mechanical model to describe the anelastic behaviour due to shear deformation and plastic flow and the Gassmann equation to take into account the fluid properties in the poro-viscoelastic model.

In this work we use this direct grid method to simulate PS seismic waves in a 2-D poro-viscoelastic model of the heterogeneous Earth's crust.

## 2. MODEL DESCRIPTION

The BDT can be viewed as the transition between zones with viscoelastic and plastic behaviour, i.e., between the upper, cooler, brittle and the deeper ductile crustal zones. Its behaviour depends on stress and temperature conditions and it is principally determined by the viscosity of the crustal rocks. The contrast in properties, at this transition, is mainly due to the different shear rigidity which is higher in the brittle medium. The medium with plastic behaviour flows when subjected to deviatoric stress, expressed by the octahedral stress, which determines the character of the flow. Figure 1 shows the octahedral stress as function of strain.

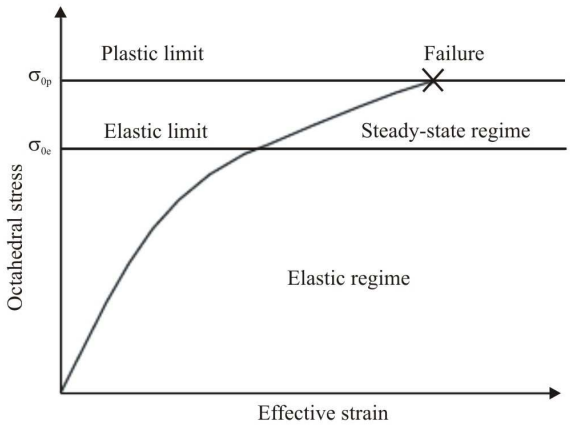


**Figure 1: Octahedral stress $\sigma_0$ as a function of strain. The rock starts to yield when $\sigma_0$ exceeds the elastic limit $\sigma_{0e}$. Steady-state flow occurs when $\sigma_0$ is between $\sigma_{0e}$ and $\sigma_{0p}$ (modified after Carcione et al. 2014).**

### 2.1 The Gassmann-Burgers mechanical model

The constitutive equation, used for the simulation algorithm, includes the viscoelastic and the plastic behaviour, and represents the generalization to the poro-elastic case of the stress-strain relation proposed by Carcione and Poletto (2013). The viscoelastic creep is described with the Burgers mechanical model (Carcione 2004), which is a series connection of a dashpot and a Zener model (Fig. 2).

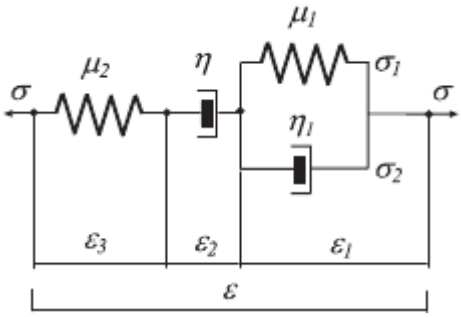


**Figure 2: Burgers mechanical model for shear deformation (Carcione 2014). σ, ε, μ and η represent stress, strain, shear modulus and viscosity, respectively. The seismic relaxation is described by $\eta_1$ and the plastic flow by η.**

The common expression in the time domain is the creep function

$$X = \left( \frac{t}{\eta} + \frac{1}{\mu_0} \left[ 1 - \left( 1 - \frac{\tau_\sigma}{\tau_\varepsilon} \right) \exp\left( t/\tau_\varepsilon \right) \right] \right) H(t), \qquad [1]$$

where H(t) is the Heaviside function, $\tau_\varepsilon$ and $\tau_\sigma$, are the seismic stress and strain relation times, respectively. They are expressed as functions of the quality factor by

$$\tau_\varepsilon = \tau_0 / Q_0 \left( 1 + \sqrt{Q_0^2 + 1} \right), \quad \tau_\sigma = \tau_\varepsilon - 2\tau_0 / Q_0 , \qquad [2]$$

where $\tau_0$ is the relaxation time such that $\omega_0 = 1/\tau_0$ is the centre frequency of the relaxation peak and $Q_0$ is the minimum quality factor (Carcione et al. 2013).

The deformation of the ductile layer is described using the octahedral stress, which is

$$\sigma_0 = \frac{1}{3} \sqrt{(\sigma_v - \sigma_h)^2 + (\sigma_v - \sigma_H)^2 + (\sigma_h - \sigma_H)^2} , \qquad [3]$$

where $\sigma_v$ is the vertical lithostatic stress, $\sigma_H$ and $\sigma_h$ are the maximum and minim horizontal stress, respectively (Carcione and Poletto 2013).

The saturated wet-rock Gassmann-Burgers poroelastic bulk and shear moduli are given by

$$K_w = K_d + \alpha^2 M \quad \text{and} \quad \mu_w(\omega) = \mu_d(\omega), \qquad [4]$$

$K_d$ and $\mu_d$ are the dry bulk and shear moduli, respectively,

$$\alpha = 1 - \frac{K_d}{K_s}, \qquad M = \frac{K_s}{1 - \varphi - K_d/K_s + \varphi K_s/K_f}, \qquad [5]$$

$K_s$ and $K_f$ are the solid and fluid bulk moduli, respectively, and φ is the porosity. The complex and frequency-dependent P- and S-wave velocities are

$$V_P = \sqrt{\frac{K_w + 4\mu_w(\omega)/3}{\rho}} \quad \text{and} \quad V_S = \sqrt{\frac{\mu_w(\omega)}{\rho}}, \qquad [6]$$

where the bulk density is

$$\rho = (1 - \varphi)\rho_s + \varphi\rho_f , \qquad [7]$$

$\rho_s$ and $\rho_f$ are the grain and fluid densities, respectively.

### 2.2 Arrhenius equation

The viscosity is related to the steady-state creep rate $\dot{\varepsilon}$ trough the Arrhenius equation

$$\eta = \frac{\sigma_0}{2\dot{\varepsilon}}, \qquad [8]$$

where $\sigma_0$ is the octahedral stress and the dislocation creep rate $\dot{\varepsilon}$ is represented by the steady state power law (e.g., Violay et al. 2012)

$$\dot{\varepsilon} = A\sigma_0^n \exp\left( -E/RT \right), \qquad [9]$$

being A $(MPa)^{-n}s^{-1}$ a material constant, n the stress exponent and E the activation energy (kJ/mole), which are experimentally determined. R = 8.3144 J/mol/°K is the gas constant and T the absolute temperature.

## 3. EQUATIONS OF MOTION

The equation of motion can be described using the Burgers relaxation function

$$\Psi(t)=\left[A_1\exp\left(-t/\tau_1\right)-A_2\exp\left(-t/\tau_{21}\right)\right]H(t), \quad [10]$$

where

$$\tau_{1,2}=-\frac{1}{\omega_{1,2}}, \quad [11]$$

are the relaxation times and

$$A_{1,2}=\frac{\mu_1\mu_2+\omega_{1,2}\eta_1\mu_2}{\eta_1(\omega_1-\omega_2)}, \quad [12]$$

are coefficients calculated using

$$(2\eta\eta_1)\omega_{1,2}=-b\pm\sqrt{b^2-4\mu_1\mu_2\eta_1\eta}, \quad [13]$$

$$b=(\mu_1+\mu_2)\eta+\mu_2\eta_1, \quad [14]$$

$$\mu_1=\frac{\mu_0\tau_\varepsilon}{(\tau_\varepsilon-\tau_\sigma)}, \quad \mu_2=\frac{\mu_0\tau_\varepsilon}{\tau_\sigma}, \quad \eta_1=\mu_1\tau_\varepsilon, \quad [15]$$

$\mu 0$ is the relaxed ($\omega = 0$) shear modulus of the Zener element ($\eta = \infty$).

### 3.1 2-D PS wave propagation

We write the stress-strain relations considering the plane-strain conditions with propagation in the (x, z)-plane, as

$$\dot{\sigma}_{xx}=K_w(\partial_x v_x+\partial_z v_z)+\frac{2}{3}\dot{\Psi}*(2\partial_x v_x-\partial_z v_z),$$
$$\dot{\sigma}_{zz}=K_w(\partial_x v_x+\partial_z v_z)+\frac{2}{3}\dot{\Psi}*(2\partial_z v_z-\partial_x v_x), \quad [16]$$
$$\dot{\sigma}_{xz}=\dot{\Psi}*(\partial_x v_z-\partial_z v_x),$$

where $v_{x,z}$ are the particle-velocity components, and $\partial_{x,z}$ the spatial derivatives. The temporal convolution, expressed by '$*$', can be overcame by using memory variables (Carcione 2014)

$$\dot{\Psi}*\partial_i v_i=A_1(\partial_i v_i+e_{ij}^1)-A_2(\partial_i v_i+e_{ij}^2), \quad [17]$$

$$\dot{e}_{ij}^{(m)}=-\frac{1}{\tau_m}(\partial_i v_j+e_{ij}^{(m)}) \quad m=1,2 \quad i,j=x,z. \quad [18]$$

The recast stress-strain relations are

$$3\dot{\sigma}_{xx}=[3K_w+4(A_1-A_2)]\partial_x v_x+[3k_w-2(A_1-A_2)]\partial_z v_z$$
$$+2(2A_1e_{xx}^{(1)}-2A_2e_{xx}^{(2)}-A_1e_{zz}^{(1)}-A_2e_{zz}^{(2)}),$$
$$3\dot{\sigma}_{zz}=[3K_w+4(A_1-A_2)]\partial_z v_z+[3k_w-2(A_1-A_2)]\partial_x v_x$$
$$+2(2A_1e_{zz}^{(1)}-2A_2e_{zz}^{(2)}-A_1e_{xx}^{(1)}-A_2e_{xx}^{(2)}), \quad [19]$$
$$\dot{\sigma}_{xz}=(A_1-A_2)(\partial_x v_z+\partial_z v_x)+A_1(e_{xz}^{(1)}+e_{zx}^{(1)})-A_2(e_{xz}^{(2)}+e_{zx}^{(2)}),$$

and the dynamical equations of motion are

$$\dot{v}_x=\frac{1}{\rho}(\partial_x\sigma_{xx}+\partial_z\sigma_{xz})+s_x,$$

$$\dot{v}_z=\frac{1}{\rho}(\partial_x\sigma_{xz}+\partial_z\sigma_{zz})+s_z, \quad [20]$$

(e.g., Carcione 2014), where $\rho$ is the bulk density defined by [6] and $s_i$ are the source components. The relations [19] and [20] can be written in matrix notation as

$$\dot{\mathbf{v}}=\mathbf{M}\cdot\mathbf{v}+\mathbf{s}, \quad \mathbf{v}=(v_x,v_z,\sigma_{xx},\sigma_{zz},\sigma_{xz},e_{ij}^{(m)})^T, \quad [21]$$

where the $13\times13$ matrix $\mathbf{M}$ contains the material properties and spatial derivatives.

## 4. EXAMPLES

We present examples that show the capability of the full-waveform simulator to seismically characterize rock rheology in the presence of very high temperatures, where supercritical fluids may be present.

We assume propagation in a homogeneous, isotropic medium under lithostatic pressure. The compressional (Vp) velocity of the medium is 6000 m/s, the shear (Vs) velocity is 3464 m/s and the density is 2700 kg/m$^3$. The material constants used to calculate the viscosity variation through the Arrhenius equation [7] and [8], are that of glass-free basalt, i.e., n = 3.5, A = 1e+30 (MPa)$^{-n}$s$^{-1}$ and the activation energy E = 990 kJmol$^{-1}$ (Violay et al. 2010). The fluid density and acoustic velocity change with pore pressure and temperature. The density and acoustic velocity of the saturating fluid (water) are calculated using CoolProp codes (Bell et al. 2014), based on NIST database (Lemmon et al. 2005), including supercritical behaviour. The hydrostatic pore pressure is given by $p_o=\rho_f*g$. We apply an iterative procedure to calculate the pore pressure. We start using an average fluid density of 1000 kg/m$^3$, then we upgrade the values using the new densities obtained for each couple temperature-pressure until the procedure converges.

To obtain the octahedral stress [2] we use a simple model based on gravity contribution at depth z (Carcione et al. 2016). The horizontal stresses can be estimated as

$$\sigma_H=\frac{\nu\sigma_v}{1-\nu}, \quad \text{and} \quad \sigma_h=\xi\sigma_H, \quad [22]$$

where $\nu$ is the Poisson ratio, $\sigma_v=-\bar{\rho}gz$ is the lithostatic stress calculated using 2400 kg/m$^3$ as average density ($\bar{\rho}$) g = 9.81 m/s$^2$ and $\xi$ = 0.8 is a parameter introduced to model additional effects due to tectonic activity.

We simulate synthetic wave propagation with three 1D temperature profiles: A vertical gradient, which starts from 20 °C at the surface and reaches 300°C at a depth of 7 km (Fig. 3a), and two step functions with

temperature that changes from 100 °C in the first 2 km depth to 800 °C below 5 km depth (Fig. 3b) and to 1200 °C below 5 km depth (Fig. 3c).

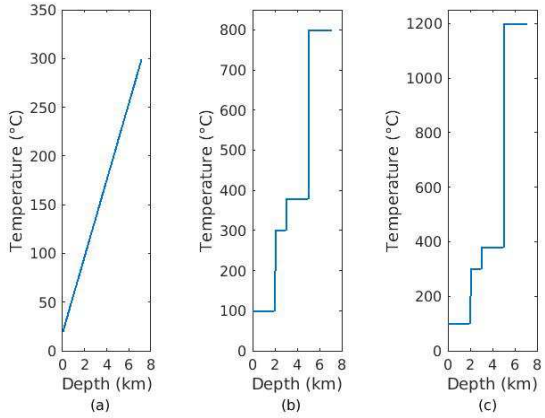


**Figure 3: 1D temperature profiles used to simulate wave propagation: (a) gradient function that reaches a maximum temperature of 300 °C at 7 km depth, (b) step function where the maximum value 0f 800 °C is reached at 5 km depth, (c) step function where the maximum value of 1200 °C is reached at 5 km depth.**

In the first example, we calculate water properties (density and bulk modulus) in the analysed depth range (0-7 km) for the 1D temperature profile of Fig. 3a. The water pore pressure, density and acoustic velocity are shown versus depth in Figs. 4a, b and c, respectively.

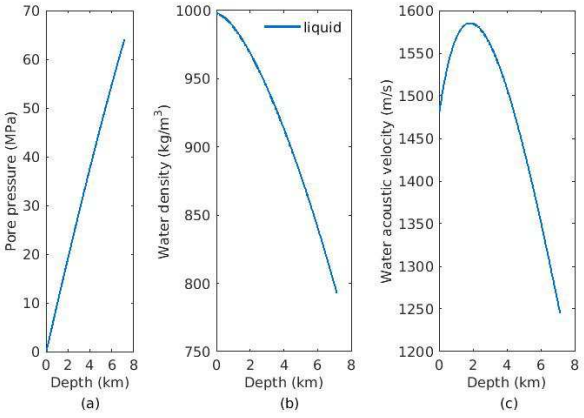


**Figure 4: Water properties calculated using NIST database, in the depth range 0 – 7 km, associated to the 1D temperature profile of Fig. 3a. (a) Pore pressure, (b) density and (c) acoustic wave velocity.**

For these selected pore pressure and temperature ranges, the pore fluid state remains liquid. We use the fluid properties and obtain seismic (phase) velocities for the wet glass-free basalt rock with 5% porosity using the analytical (plane-wave) calculation (Carcione et al. 2016). The behaviour of phase velocities (Vp and Vs) and their ratio, are shown in Figs. 5a, b and c, respectively as function of depth, for the wet glass-free basalt rock with 5% porosity.

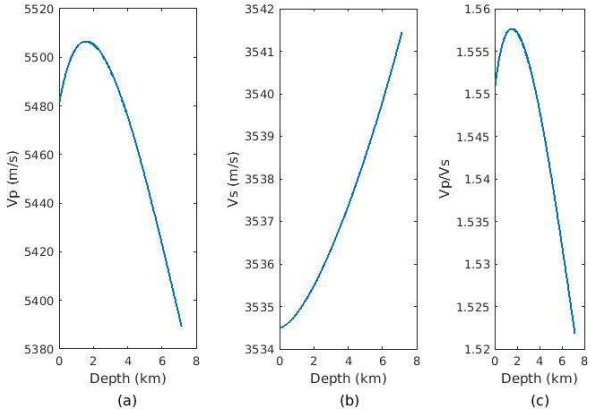


**Figure 5: Phase velocities (a) Vp, and (b) Vs, and (c) their ratio as function of depth, for the wet glass-free basalt rock, with 5% porosity, in the depth range 0 – 7 km, associated to the temperature profile of Fig. 3a.**

We then calculate the synthetic propagation with the full-wave numerical algorithm, based on the Fourier pseudospectral method using the fluid and rock properties associated to the temperature profile of Fig. 3a. We consider a model with dimensions 6 x 7 km, discretized with squared pixel with sides of 15 m. We implement a source in the center of the model at 900 m depth. The source signal is a Ricker wavelet with a central frequency of 50 Hz. We record the vertical and the horizontal particle velocity components of a zero-offset VSP when we use a vertical force and a horizontal force, as source, respectively. The zero-offset VSP (vertical component) recorded when a vertical force is used, is shown in Fig. 6a, while the horizontal component recorded when the horizontal force is used, can be observed in Fig. 6b.

In these examples, we assume as an approximation water as geothermal fluid. The critical temperature and pressure for water, above which we find supercritical conditions, are 373.946 °C and 22.064 MPa, respectively. If we use the temperature profile of Fig. 3b, we have supercritical fluid below 3 km depth. Figs. 7a, b and c show pore pressure, density and acoustic velocity, respectively, for water when the temperature changes as in Fig. 3b in the depth range 0 – 7 km. The different fluid-phase conditions are denoted by different colours, blue for liquid and green for supercritical phase.

Using the fluid properties, with the analytical (plane-wave) calculation, we obtain Vp and Vs velocities and their ratio for the wet free-glass basalt rock with 5% porosity. The results are shown in Figs. 8. The wet rock phase velocities change according to the temperature and the reflections due to these changes can be observed in the simulated VSPs (Figs. 9a, b). In particular, the yellow arrows indicates the reflections

due to the presence of supercritical fluid, below the depth of 3 km.

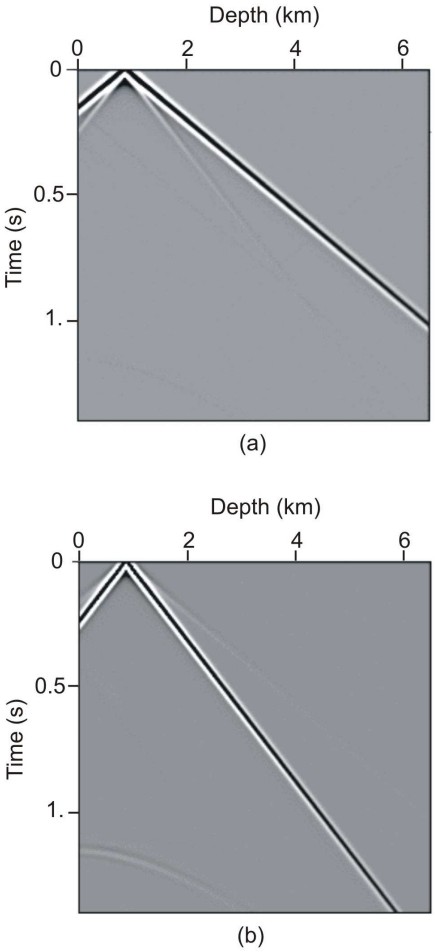


**Figure 6: Zero-offset VSP (a) vertical particle velocity component with vertical force as source, (b) horizontal particle velocity component with horizontal force as source.**

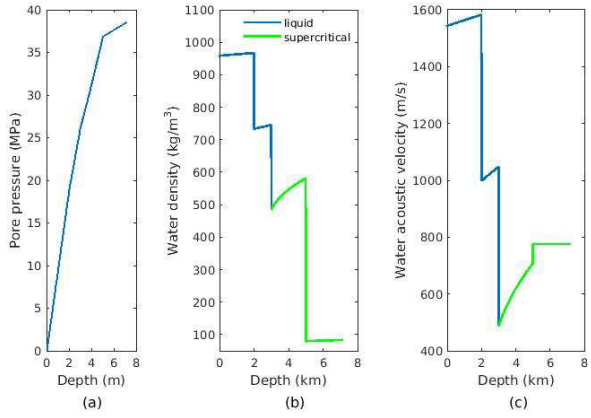


**Figure 7: Water properties calculated using NIST database, in the depth range 0–7 km, associated to the temperature profile of Fig. 3b. (a) Pore pressure, (b) density and (c) acoustic wave velocity. Values in blue are associated to the water liquid state and in green to the supercritical state.**

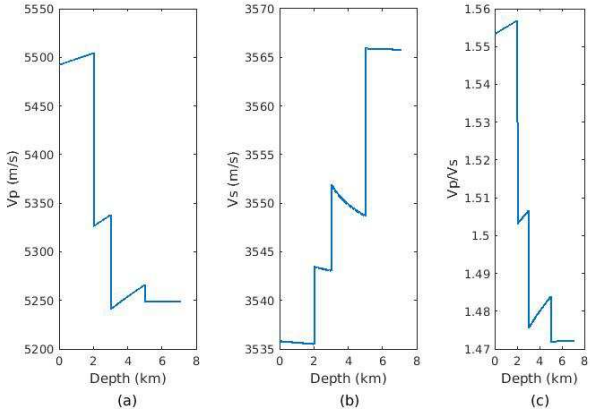


**Figure 8: Phase velocities (a) Vp and (b) Vs, and (c) their ratio as function of depth, for the wet glass-free basalt rock, with 5% porosity, in the depth range 0 – 7 km, associated to the temperature profile of Fig. 3b.**

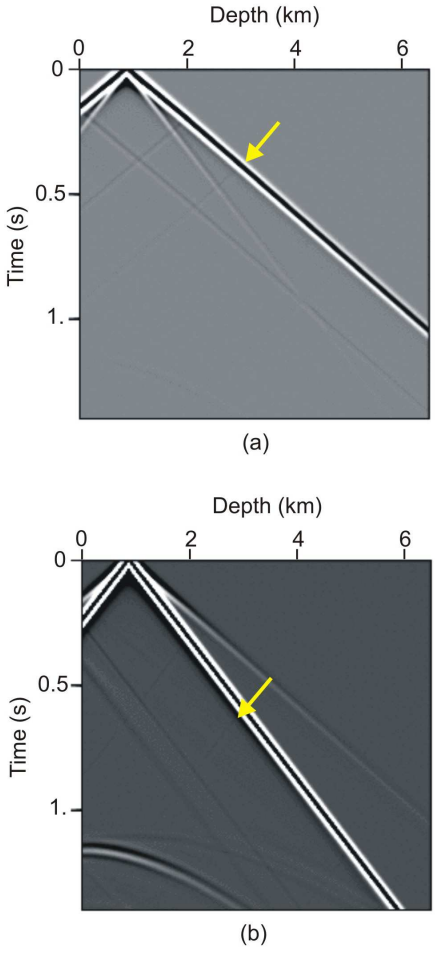


**Figure 9: Zero-offset VSP (a) vertical particle velocity component with vertical force as source and (b) horizontal particle velocity component with horizontal force as source using a medium with 5% porosity. The reflections due to the presence of supercritical fluid are shown by the yellow arrows.**

We calculate the Vp-wave velocity by picking synthetic data of Fig. 9a. In the range depth up to 2 km, where T = 100 °C, Vp = 5555 m/s, between 2 and 3 km, where T = 200 °C, Vp = 5340 m/s, between 3 and 5 km, where T = 380 °C and supercritical water is present Vp = 5261 m/s. Below 5 km depth, where T = 800 °C and there still is supercritical water Vp = 5254 m/s. These velocity values agrees with the analytical results shown in Fig.8a. The Vs-wave velocity variation observed in Fig. 8b is not appreciable by the picking of synthetic data of Fig. 9b. The Vs measured from synthetic seismogram is 3550 m/s in all the depth ranges.

We then model the same temperature profile (Fig. 3b) in the presence of dry rock. In this case the analytically calculated seismic velocities (Vp and Vs) do not change (Figs. 10a and b) with temperature. The VSPs simulated with the presence of dry rock and the temperature profile of Fig. 3b are shown in Fig. 11. The Vp and Vs calculated by picking synthetic data of Figs. 11a and b, respectively, are Vp = 6020 m/s and Vs = 3484 m/s, values that agrees with the analytical ones.

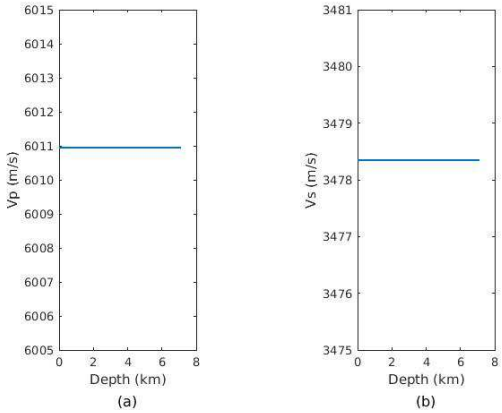


**Figure 10: Phase velocities (a) Vp and (b) Vs, as function of depth, for glass-free basalt rock without fluid, in the depth range 0–7 km, associated to the temperature profile of Fig. 3b.**

The last example is calculated to show the capability of the presented simulator to seismic characterize the brittle-ductile transition. For this reason we choose the temperature profile shown in Fig. 3c, where below the depth of 5km the temperature reaches 1200 °C. The medium is modelled with wet free-glass basalt rock with 5% porosity until 5 km depth and dry-free-glass basalt rock for deeper depth. When the temperature reaches 1200 °C, the dry rock melts and its phase velocities drastically changes (Fig. 12). The vertical particle velocity component of the vertical seismogram recorded when a vertical force is applied, is shown in Fig. 13 where the yellow line indicates the depth at which rock starts melting (5 km).

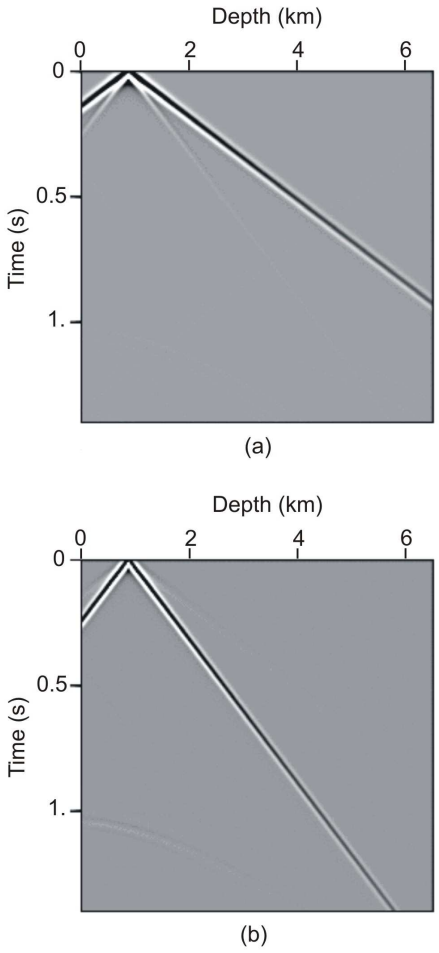


**Figure 11: Zero-offset VSP (a) vertical particle velocity component with vertical force as source and (b) horizontal particle velocity component with horizontal force as source using dry medium.**

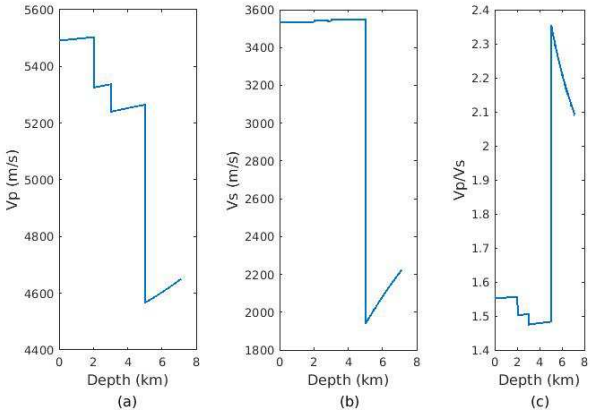


**Figure 12: Phase velocities (a) Vp and (b) Vs, and (c) their ratio as function of depth, for the wet glass-free basalt rock, with 5% porosity until 5 km depth and dry rock below, in the depth range 0–7 km, associated to the temperature profile of Fig. 3c.**

We measure the P-wave velocity by picking data and we observe that Vp varies in the correspondence of temperature changes. In the range depth up to 2 km, where T = 100 °C, Vp = 5555 m/s, between 2 and 3 km, where T = 200 °C, Vp = 5340 m/s, between 3 and 5 km, where T = 380 °C and supercritical water is present Vp = 5261 m/s. Below 5 km, when the temperature reaches 1200 °C, the fluid is no still present and the dry rock melt, we register a drastic decreasing of the velocity and Vp = 4510 m/s. The Vp values obtained by picking synthetic data agree with the analytic phase velocity shown in Fig. 12a.

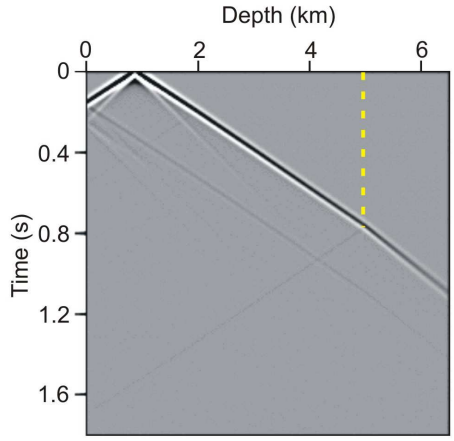


**Figure 13: Zero-offset VSP (a) vertical particle velocity component with vertical force as source and using the temperature profile of Fig. 3c. The yellow line indicates the depth of 5 km where melting starts.**

## 5. CONCLUSIONS

We present a full-waveform algorithm to model the seismic properties of crust and mantle rock as function of in-situ temperature and pressure. The methodology, which is based on the Burgers viscoelastic model and Gassmann modulus, takes into account the effects of temperature and pressure on the saturating fluids, including supercritical conditions, and on the rock frame, including melting. Since the approach is based on Gassmann equation, we explicitly obtain the wet-rock seismic velocities as a function of the fluid bulk modulus. The examples illustrate the capability of the simulator to retrieve temperature from seismic velocities in the presence of fluid, including supercritical behaviour. The examples show that the discontinuity at which supercritical condition appears can be seismically observable. The wet-rock P-wave velocity obtained from full-wave data decreases from 5550 m/s at T = 100°C to 5260 m/s at T=800°C, in agreement with the analytical (plane-wave) calculations. Melting can be detected as well, since the wet-rock P-wave velocity decrease from 5550 m/s at T = 100 °C to 4510 m/s at T = 1200 °C for dry melted rock.

## REFERENCES

Bell, I.H., Wronski, J., Quoilin, S. and Lemort, V.: Pure and pseudo-pure fluid thermophysical property evaluation and the open-source thermophysical property library CoolProp. *Ind. Eng. Chem. Res.*, **53** (6), 2498–2508, (2014).

Carcione, J.M.: Wave fields in real media: Wave propagation in anisotropic, anelastic, porous and electromagnetic media. Handbook of Geophysical Exploration, vol. 38, *Elsevier*, (2014).

Carcione, J.M. and Poletto, F.: Seismic rheological model and reflection coefficients of the brittle-ductile transition, *Pure and Applied Geophysics*, **170** (2), (2013), 2021-2035.

Carcione, J.M., Poletto, F., Farina B. and Craglietto, A.: Simulation of seismic waves at the Earth crust (brittle-ductile transition) based on the Burgers model, *Solid Earth*, **5**, (2014), 1001-1010.

Carcione, J.M., Poletto, F., Farina, B. and Craglietto, A.: The Gassmann-Burgers model to simulate seismic waves at the Earth crust and mantle, *Submitted to Pure and Applied Geophysics*, 2016.

Lemmon, E.W., McLinden, M.O. and Friend, D.G.: Thermophysical properties of fluid systems. NIST Chemistry Webbok 69, NIST Standard Reference Database, *Lindstrom P.J. and Mallard W.G. eds.*, Gaithersburg, (2005).

Poletto, F. and Miranda, F,: Seismic while drilling. Fundamentals of drill-bit seismic for exploration. Handbook of Geophysical Exploration, vol. 35, *Elsevier*, (2004).

Violay, M., Gibert, B., Mainprice, D., Evans, B., Pezard, P.A., Flovenz, O.G. and Asmundsson, R.: The brittle-ductile transition in experimentally deformed basalt under oceanic crust conditions: Evidences for presence of permeable reservoirs at supercritical temperatures and pressures in the Icelandic crust. *Proceedings of the World Geothermal Congress 2010*, Bali, Indonesia, (2010).

Violay, M., Gibert, B., Mainprice, D., Evans, B., Dautria, J.M., Azais, P. and Pezard, P.A.: An experimental study of the brittle-ductile transition of basalt at oceanic crust pressure and temperature conditions. *Geophy. Res.*, **117**, (2012), 1-23.